JOURNAL OF PROPULSION AND POWER
Vol. 9, No. 1, Jan.–Feb. 1993

Influences on the Sprays Formed by High-Shear Fuel Nozzle/Swirler Assemblies

J. M. Cohen* and T. J. Rosfjord†
United Technologies Research Center, East Hartford, Connecticut 06108

A high-shear nozzle/swirler (HSNS) consists of a centrally mounted fuel nozzle in a compound, radial inflow air swirler. The first part of this study focuses on the influences of the swirler design parameters and fuel injection technique on the uniformity, solidity, and cone angle of the produced spray. High resolution patternation data and airflow data were acquired for 21 different nozzle/swirler configurations. The second part of the study investigates the effects of manufacturing and assembly defects on the uniformity of the sprays. High resolution patternation data were collected for three groups of perturbations to a baseline assembly. Data were compared on the basis of radial and circumferential fuel flux distributions.

Introduction

THE fuel injection process is critical to achieving the full potential of a gas turbine engine. Liquid fuel must be atomized and distributed in an airstream to achieve a certain range of combustible mixtures. If either the atomization or the distribution is poor, extremely fuel-rich regions will be produced. Unacceptably high levels of incompletely oxidized carbon compounds will be produced, resulting in reduced combustion efficiency and excessive smoke emissions. More finely atomized fuel, uniformly distributed in the airstream, will alleviate these problems. Achieving such goals, however, may compromise the combustion stability of the burner; fully uniform fuel-air mixtures will often be below the fuel flammability limits. Consideration of the fuel injection process must then include concerns both for fuel atomization and distribution and for the structure of the flowstream produced by the fuel injection device.

Most modern gas turbine combustors use aerating fuel injection systems. For these the level of fuel atomization and extent of fuel distribution depends on the dynamics of swirling airstreams. A common embodiment of this concept is the airblast fuel nozzle which delivers inner and outer swirling airstreams on either side of a thin annular sheet of fuel. Such a nozzle is usually mounted in an axial flow swirler as shown in the assembly of Fig. 1. In addition to the above roles, the nozzle and swirler airflows establish the flowfield downstream of it. For many applications, the swirl is sufficiently strong to produce a midstream flow recirculation which strongly contributes to the burner stability and ignitability characteristics. Several studies have documented the nature of flows produced by either axial flow swirlers alone[1–5] or airblast nozzles alone.[6–8]

It is clear that complex flowfields are produced downstream of aerating fuel injection systems. Since a complete understanding of a single swirling flow or its interaction with another gas or liquid flow is not known, it is not surprising that alternative aerating approaches have been used. Such approaches attempt to produce flowfield structures more suited for the application. The techniques may afford the opportunity to control the structure produced.

One aerating fuel injection technique entrusts the fuel atomization and distribution processes entirely to the air swirler. In this approach, the fuel injector acts to distribute the fuel onto a surface of the swirler, producing a fuel film which is subsequently sheared by the swirler airstreams. This is the principle of the nozzle/swirler combination depicted in Fig. 2. This combination will be referred to as a high-shear nozzle/swirler (HSNS). It consists of a fuel nozzle and a compound radial inflow swirler. The fuel nozzle can take a variety of forms, pressure atomizing, aerating, or hybrid. The swirler design produces inner and outer swirling flows using multiple inlet slots distributed around its circumference. In this manner, the magnitude and initial swirl angle of the flow are more easily controlled than for an axial flow swirler. Previous studies[9] have shown that high levels of fuel atomization can be achieved with this nozzle/swirler. Furthermore, based on results using a single nozzle combustion rig, the combustion stability (i.e., lean blowout fuel-air ratio) depended on the percentage of airflow in each passage and the respective swirl strengths (i.e.,

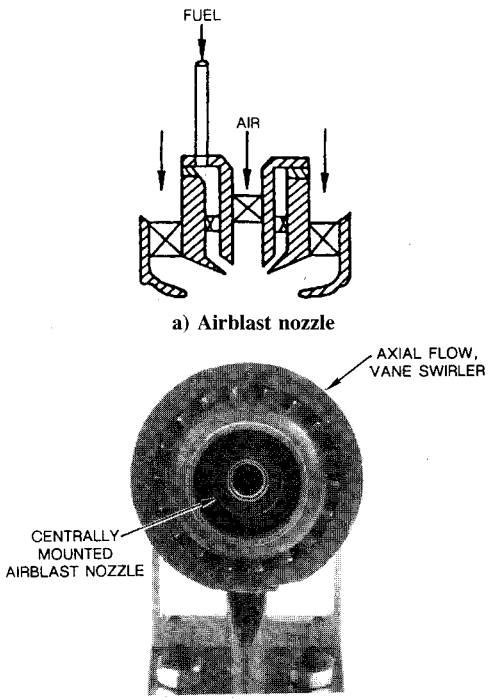

a) Airblast nozzle

b) Airblast nozzle in axial flow air

Fig. 1 Airblast atomizer using axial flow air swirler.

Presented as Paper 90-2193 at the AIAA/SAE/ASME/ASEE 26th Joint Propulsion Conference, Orlando, FL, July 16–18, 1990; received July 30, 1991; revision received June 10, 1992; accepted for publication June 25, 1992.

*Associate Research Engineer. Member AIAA.
†Senior Project Engineer. Associate Fellow AIAA.

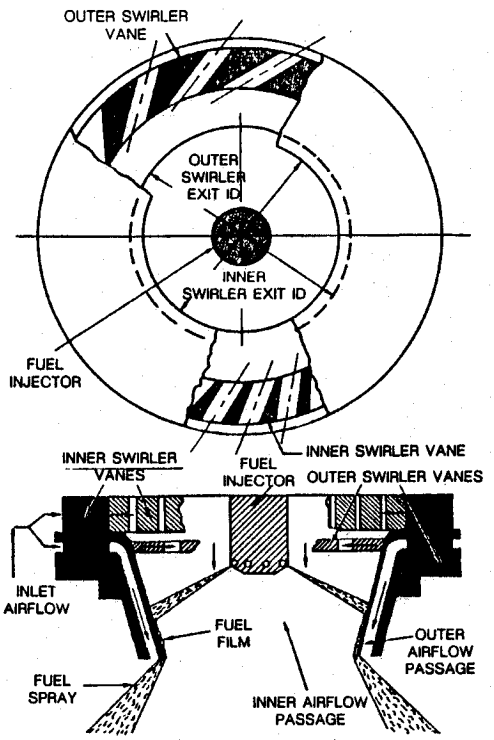

Fig. 2 High-shear nozzle–swirler operation.

swirl angles). Presumably different flowfield structures were produced downstream of the devices for these variations.

This study focused on the sensitivity of the sprays created by high-shear fuel nozzles to two types of influences: 1) those intended by the design of the device; and 2) those arising from manufacturing and assembly nonuniformities. The tests were performed with jet A fuel at a typical high power operating condition scaled to atmospheric temperature and pressure.

In the first part of the study, the effect of variation in key design parameters was gauged by testing 21 configurations assembled using 3 fuel nozzle types and 7 swirler designs. Detailed spray patternation data were acquired for all configurations. Analytical and experimental evaluations of the air swirlers were also performed. The air velocity profiles near the exit of one configuration were measured and compared to a simple model of the swirler flowfield. The sensitivity of spray character to the injection technique and swirler design are discussed.

In the second part of the study, the effects of manufacturing defects and misassembly were measured for one fuel nozzle and air swirler type. It has been shown in previous studies[10] that for airblast nozzles, such as the one shown in Fig. 1, small perturbations to the nozzle assembly caused large nonuniformities in the spray pattern. Small defects and eccentricities were introduced in a controlled fashion, and the resulting spray pattern was compared to the spray from a baseline nozzle that was properly assembled. It was found that nonuniformities in the fuel passage created the largest deviations from the baseline spray, whereas perturbations to the air swirlers caused smaller defects. High-shear devices rely on the same delicate balance of fuel and airflows that airblast nozzles do, and therefore, may also be susceptible to such behavior. Defects were imposed on a baseline assembly, which without defects, exhibited good spray uniformity characteristics. The magnitude of the perturbations was within the limits of defects often seen in manufacturing and assembly processes. Spray patternation data were collected in all cases.

Model Nozzle/Swirler

Part 1: Design Influences

The HSNS models consisted of a fuel nozzle engaged on the centerline of a compound, radial inflow air swirler. Three fuel nozzle types were used to span a range of fuel injection techniques: 1) radial jet nozzle, 2) duplex nozzle, and 3) airblast nozzle. The radial jet nozzle injected fuel by means of six circular orifices around the circumference of the nozzle tip. The orifices were canted 45 deg to the tip axis to add a downstream axial component to the fuel velocity vector. No swirl was imposed on the fuel flow. The duplex nozzle produced a hollow cone fuel spray with a nominal included cone angle of 60 deg. The airblast nozzle was similar to that previously studied.[6]

Seven compound radial inflow swirlers were designed, fabricated, and evaluated with each fuel nozzle. A compound swirler consisted of two conical elements, each admitting an airflow through multiple equivalent slots which fed a common exit (Fig. 2). When assembled the two elements were concentrically aligned, providing a circular exit for the primary flow and a thin annulus for the secondary flow. All swirler swirl was counterclockwise. The seven swirler designs were specified to represent inner swirl angles of 40, 50, or 60 deg, an outer swirl angle of 70 deg, inner/outer mass flow splits of 0.85/0.15 or 0.60/0.40, and total effective flow areas of 0.5 in.^{2} or 0.25 in.^{2} Table 1 provides the specific combinations of these parameters for the seven specified swirler designs. The geometrical specifications came from the use of a computer code based on two conservation laws: 1) mass flow, and 2) angular momentum, with the specification of empirical constants (e.g., slot discharge coefficient) based on previous experimental results. Tables 2 and 3 provide the necessary design specifications, referenced to an appropriate figure. Each swirler was fabricated from aluminum using numerically controlled machining. As an example, Fig. 3 shows the two components of swirler 1. The nozzle was inserted into the swirler through a plate covering the circular open area of the inner swirler. When assembled, selected spacers were used to achieve a 0.65-in. separation between the nozzle tip and swirler exit for all nozzle/swirler combinations.

Part 2: Manufacturing and Assembly Influences

The baseline model consisted of the radial jet, pressure atomizing fuel nozzle mounted on the centerline of a radial inflow air swirler (swirler 1). Several sets of identical swirlers were created to allow the introduction of independent defects. The fuel nozzle was inserted into the swirler through a plate covering the circular open area of the inner swirler. When assembled, the baseline separation between the nozzle tip and swirler exit was 0.65 in. Table 1 provides the appropriate design information for the air swirler used.

Test Facility

All tests were performed in a spray facility which offered the capability to economically characterize the sprays formed by fuel nozzles. It consisted of a computer-positioned plenum mount for the nozzle, a receiver tank containing a high resolution patternator, and the necessary controlling and metering devices for air and primary/secondary fuel flow rates. The test nozzle was mounted on the bottom end of the plenum and sprayed downward into the receiver. Airflow for aerating

Table 1 Design parameters for high-shear swirlers

	Airflow rate			Exit swirl	
Swirler configuration	Total C_dA, in.^{2}	Inner, %	Outer, %	Inner, deg	Outer, deg
1	0.5	85	15	60	70
2	0.5	85	15	50	70
3	0.5	85	15	40	70
4	0.5	70	30	60	70
5	0.5	70	30	50	70
6	0.5	70	30	40	70
7	0.5	70	30	40	70

Table 2 Inner radial inflow swirler design

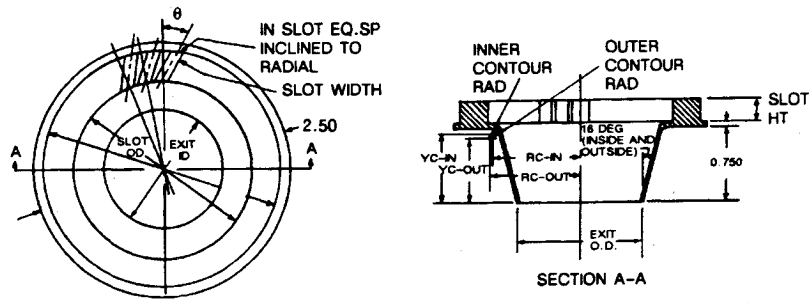

Swirler	1	2	3	4	5	6	7
Slot i.d., in.	1.86	1.86	1.86	1.64	1.64	1.64	1.42
Slot o.d., in	2.40	2.40	2.39	2.21	2.20	2.20	1.98
No. of slots	32.0	32.0	32.0	24.0	24.0	24.0	16.0
Slot angle, theta, deg	30.0	18.5	13.0	34.0	20.0	15.0	15.0
Slot height, in.	0.220	0.180	0.150	0.220	0.200	0.180	0.178
Slot width, in.	0.125	0.125	0.125	0.130	0.130	0.130	0.130
Exit i.d., in.	1.180	1.980	0.860	1.940	0.840	0.760	0.530
Exit o.d., in.	1.242	1.042	1.922	1.002	1.902	1.822	0.592
Inner contour radius, in.	0.10	0.10	0.20	0.10	0.10	0.20	0.20
YC-in, in.	0.71	0.71	0.61	0.71	0.71	0.61	0.61
RC-in, in.	0.88	0.78	0.80	0.76	0.71	0.75	0.64
Outer contour radius, in.	0.10	0.10	0.20	0.10	0.10	0.20	0.20
YC-out, in.	0.65	0.65	0.55	0.65	0.65	0.61	0.55
RC-out, in.	0.90	0.80	0.82	0.78	0.73	0.77	0.65

Table 3 Outer radial inflow swirler design

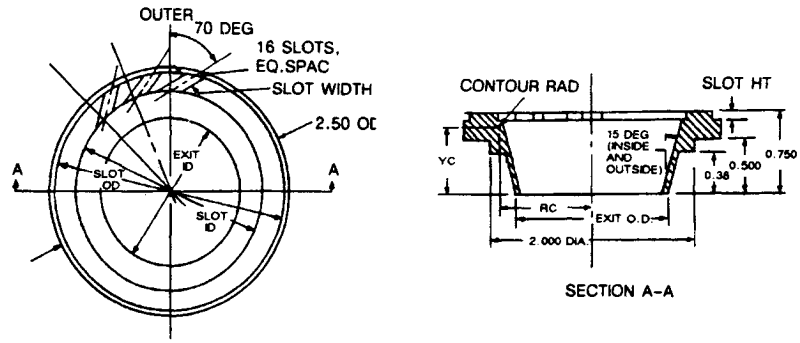

Swirler	1	2	3	4	5	6	7
Slot i.d., in.	1.86	1.86	1.86	2.00	2.00	2.00	1.86
Slot o.d., in	2.34	2.34	2.34	2.47	2.47	2.47	2.29
Slot height, in.	0.070	0.080	0.808	0.190	0.190	0.200	0.155
Slot width, in.	0.115	0.115	0.115	0.115	0.115	0.115	0.105
Exit i.d., in.	1.380	1.180	1.100	1.380	1.280	1.230	0.820
Exit o.d., in.	1.504	1.304	1.224	1.504	1.404	1.354	0.944
Outer contour radius, in.	0.05	0.10	0.20	0.10	0.10	0.20	0.20
YC-out, in.	0.63	0.57	0.47	0.46	0.35	0.35	0.40
RC-out, in.	0.91	0.85	0.88	0.92	0.87	0.92	0.72

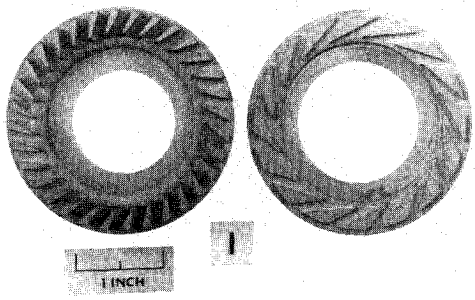

Fig. 3 Top view of inner and outer swirler components.

nozzles was fed to the plenum; fuel lines were plumbed through the plenum to the nozzle.

A unique feature of the facility was the high resolution patternator. This system and its operation have been previously described in detail.[8] In brief, the system consisted of a "wagon-wheel" array of probes which feed liquid collection devices. The patternator rake contained 60 tubes, 10 each on six equally-spaced radii within a 4-in. diam. The plenum was positioned above the patternator to place the injector axis at the center of the rake. The separation distance between the nozzle and rake was either predetermined or adjusted so that the rake intercepted an entire cross section of the spray cone. Liquid collected by a probe accumulated in a cylinder with the quantity determined by changes in liquid column pressure

in the cylinder as sensed by a Scanivalve ZOC electronic transducer. A schematic of the patternator is shown in Fig. 4.

The patternation process was automated and controlled by an Apple IIe computer. Initially, the fuel and airflows were established with covers over the collection tubes. The computer recorded initial readings on each ZOC. Upon initiation of patternation the covers were withdrawn. The computer monitored each collector and terminated the process by returning the covers at a set point collection volume. After a 1-min pause to assure complete drainage into the cylinder, ZOC readings were acquired and by means of calibration factors and the initial reading, were used to compute the local mass flux. An ejector system was actuated to empty each cylinder and a new zero ZOC reading was acquired. At this point, the computer could reposition the plenum and repeat the entire process. Typically, the plenum was rotated to cover the spray in 10-deg increments, providing 360 points of spray mass flux. Data were saved on floppy disks and later transferred to an Apollo DN4000 computer. Subsequent processing yields information on averaged circumferential and radial spray distributions, cone angles, and spray contours.

The detailed spray patternation data were processed and analyzed in a manner previously described.[8] The 360 measurements of local fuel flux were processed to produce contour plots (two-dimensional representations with lines of constant mass flux), three-dimensional projections of these contours, a radial mass flux profile obtained by averaging the 36 data at a common radius, and a sector analysis. The latter integrated the mass flux data to evaluate the circumferential uniformity of the spray. In particular, the quantity of the spray contained in a 45-deg flow sector was evaluated, with the normalized maximum deviation from the average [denoted: (Max-Ave)/Ave] used as an indicator of nonuniformity. The "error bars" or the radial profile indicate azimuthal variations at each radius. Figure 5 shows sample results.

A spray cone angle was computed from the mass flux data by integrating them outward from the centerline until 90% of the total mass flow was accounted for. The radius at this location and the downstream sampling location defined one half of the "90% spray angle." For sprays originating from a finite diameter (i.e., not a point) the radius of the source was included to provide a cone angle representing the spray expansion beyond the source diameter. All cone angles were measured from the inner diameter of the filming surface (inner swirler). This reference accounted for the effects of different filming diameters in the cone angle calculations.

The test conditions for ambient spray tests were scaled from nominal engine operating conditions. The velocity of the air through the nozzle/swirler was matched, and the fuel flow set at the value required to match the air/fuel momentum ratio of the engine condition. This procedure, preserving momentum ratio and shear, scaled mechanisms believed to be important for atomization and patternation, especially for airblast-type injectors. Detailed patternation data were acquired 2-in. downstream of each model nozzle configuration. The scaled high-power operating condition for the HSNS was

Fuel flowrate = 240 lbm/hr
Swirler airflow pressure loss = 2.25 psid

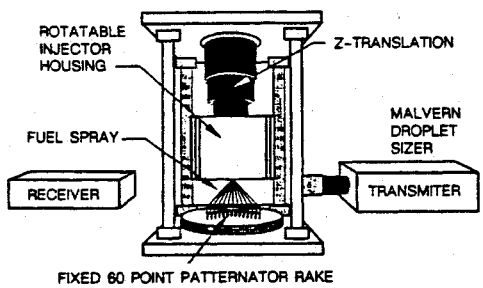

Fig. 4 High-resolution spray patternator.

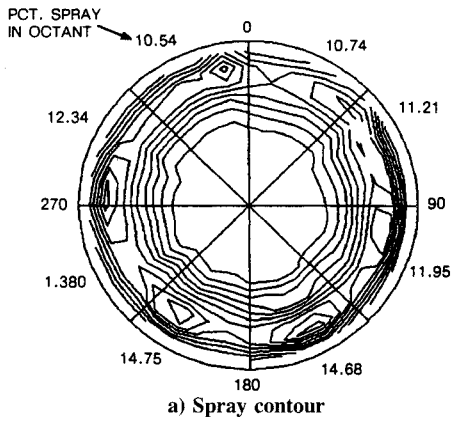

a) Spray contour

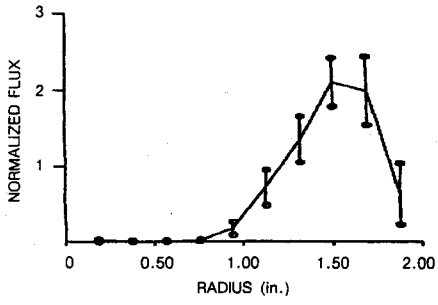

b) Radial profile

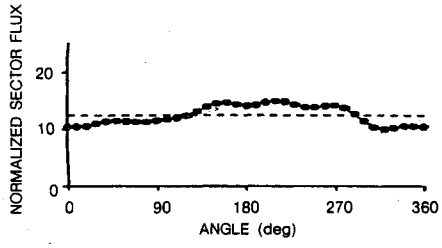

c) Sector flux

Fig. 5 Sample spray patternation data.

Results, Part 1: Design Influences

Swirler Flow Evaluations

The seven, compound radial-inflow swirlers were designed to achieve certain airflow capacity, flow split, and swirl angle goals. Flow checks of the manufactured items were performed to determine whether these goals were achieved.

The swirler airflow checks were performed with each swirler installed in the plenum of the ambient spray facility and discharging to atmospheric pressure. The inner and outer swirlers were assembled with epoxy cement using a fixture capturing their outer diameters and thus assuring component concentricity. The nozzle mounting hole was plugged. For each swirler, the mass flow (as metered by a choked venturi) and the associated swirler pressure drop were recorded for two air settings. The measurements were acquired for the inner swirler alone (as achieved by plugging the outer swirler inlet slots) and for the complete swirler assembly. The flow characteristics of the outer swirler were obtained as the difference between the total assembly and inner swirler values. The data permitted calculation of the effective area (C_dA) for each flow circuit and the assembly, and therefore, calculation of the percentage of the total airflow through each passage. Assuming that the radial velocity at the exit was small, and that the dump loss at the exit of each flow path dominated the measured pressure drop, an exit swirl angle could also then be computed. In particular, the swirl velocity acted to reduce the geometrical exit area (A) to an effective area. That is, the total mass was conserved

$$U_T^* C_d A = U_Z^* A$$

Table 4 Measured flow properties of radial inflow swirlers

Swirler assembly	1	2	3	4	5	6	7
Inner swirler							
C_dA, in.^{2}	0.475	0.409	0.370	0.288	0.328	0.301	0.171
Swirl angle, deg	64	57	50	65	54	49	40
Recalculated swirl angle, deg	57	44	30	60	43	35	27
Airflow, percent of total	91	85	83	63	66	58	67
Outer swirler							
C_dA, in.^{2}	0.047	0.070	0.071	0.169	0.196	0.213	0.082
Swirl angle, deg	80	73	76	76	72	71	70
Total assembly							
C_dA, in.^{2}	0.52	0.48	0.44	0.46	0.52	0.51	0.25

where

U_T = total velocity vector magnitude at exit
U_Z = axial velocity component at exit

The swirl of the flow may be quantified as follows:

$$\cos\theta = U_Z/U_T = C_dA/A = C_d$$

where

θ = effective exit swirl angle

This approach was followed to calculate the values presented in Table 4.

To aid in the interpretation of the airflow check data and calculations, a simple mathematical model was formulated for a radial inflow swirler. Each passage was assumed to be independent, excepting that both experienced the same total pressure loss. The model was based on conservation of mass flow and axial flux of angular momentum for a constant density flow. Equating inlet and exit flows yields

$$\text{Mass:} \quad N_S^*(C_dA)_S^*U_S = \int U_Z^* \, dA_E$$

$$\text{Momentum:} \quad R_0^*U_S^{2*}(C_dA)_S^* \sin\alpha = \int U_Z^*U_\theta^*r^* \, dA_E$$

where

N_S = number of inlet slots
$(C_dA)_S$ = effective flow area of each inlet slot, $C_d = 0.8$
U_S = mean velocity in each slot
R_0 = radial distance to inlet slot discharge
U_Z = axial velocity component at exit
U_θ = tangential velocity component at exit
α = angle between slot axis and radius of swirler ($\alpha = 0$ denotes radial flow)
dA_E = area element at swirler exit
r = radial distance for integration

The calculated total pressure loss was the sum of the jet dynamic head exiting an inlet slot and the dynamic head of the flow exiting the swirler. For the assumed exit velocity profiles for U_Z and U_θ, the inlet velocity and pressure loss contributions can be calculated. For each swirler design, inlet primary and secondary swirler velocities were determined which matched the pressure loss through both circuits to the ambient test condition loss of 2.25 psid. The system of governing and auxiliary equations were solved using a personal computer spreadsheet program.

Swirler flows corresponding to two exit velocity profiles were evaluated for the inner swirler. First, both axial velocity and tangential velocity profiles were assumed to be uniform. In this case, the effective moment arm for the velocity becomes $\frac{2}{3}$ the exit radius, and the tangential velocity is

$$U_\theta = \tfrac{3}{2}(R_0/R_E)U_S \sin\alpha$$

As R_E decreases, U_θ increases. However, U_Z increases as R_E^{-2}. The swirl angle (constant over the exit area) then decreases with reduced exit area since

$$\theta = \tan^{-1}(U_\theta/U_Z) \sim \tan^{-1}(R_E)$$

An assumed uniform U_θ profile presents a flow discontinuity at the centerline.

The second set of assumed exit velocity profiles corresponded to uniform axial flow and solid body rotation. In this case

$$U_\theta = U_{\theta,\max}(r/R_E)$$

Matching inlet and exit angular momentum yields

$$U_{\theta,\max} = 2(R_0/R_E)U_S \sin\alpha$$

or tangential velocities greater than the one-dimensional value for $r/R_E > 0.75$. The swirl angle (a function of radius) will also be greater in this region. The outer swirler exit was a relatively thin annulus; uniform axial and tangential velocity components were assumed.

Table 5 presents results from the radial-inflow swirler model for both sets of velocity profile assumptions. Included are predictions for the percentage of the total airflow passing through the primary swirler, both swirl angles, the total flow capacity, and the percentage of the entire pressure loss experienced at the swirler exit. The first four of these quantities are also depicted in Fig. 6 along with the corresponding values determined from the flow check tests. In general, the model predictions matched the properties from the flow check measurements. For global features such as airflow split and total C_dA, predictions from either velocity profile assumption were essentially equivalent; the outer swirl angle predictions were mathematically identical. The inner swirl angle derived from a flow check measurement was better tracked by the prediction using the solid body rotation tangential velocity profile. In this case, U_θ (and hence θ) was a function of radial position; the maximum q value (which occurred at the filming surface) are plotted.

Data were acquired for swirler no. 1 using a single component aerometrics phase Doppler particle analyzer (PDPA). This instrument extends the concept of laser velocimetry to permit the determination of particle velocity and size in a small measurement volume. Data were acquired with the radial jet nozzle delivering a very low fuel flow rate to act as an airflow seed. The PDPA was mounted on the receiver tank of the spray facility, and the plenum containing the swirler traversed to obtain an airflow velocity profile across a diameter. Two traverses were performed (once to determine

Table 5 Model predictions for radial inflow swirlers

Swirler assembly	1	2	3	4	5	6	7
Uniform exit velocity profiles							
Inner airflow, %	87	86	85	66	68	66	67
Swirl Angle—inner, deg	61	50	41	62	48	40	38
—outer, deg	75	73	76	76	76	76	71
C_dA total, in.^{2}	0.48	0.43	0.38	0.43	0.44	0.41	0.23
DP at exit—inner, %	64	58	55	73	64	63	74
—outer, %	66	73	76	72	76	78	87
Solid body rotation profile							
Inner airflow, %	88	86	85	66	69	67	67
Swirl angle—inner, deg	68	58	50	68	56	48	46
—outer, deg	75	73	76	76	76	76	71
C_dA total, in.^{2}	0.49	0.44	0.39	0.44	0.44	0.42	0.23
DP at exit—inner, %	68	61	56	78	67	65	77
—outer, %	66	73	76	72	76	78	87
Linear axial and tangential profile							
Swirl angle—inner, deg	57	44	35	57	42	34	31

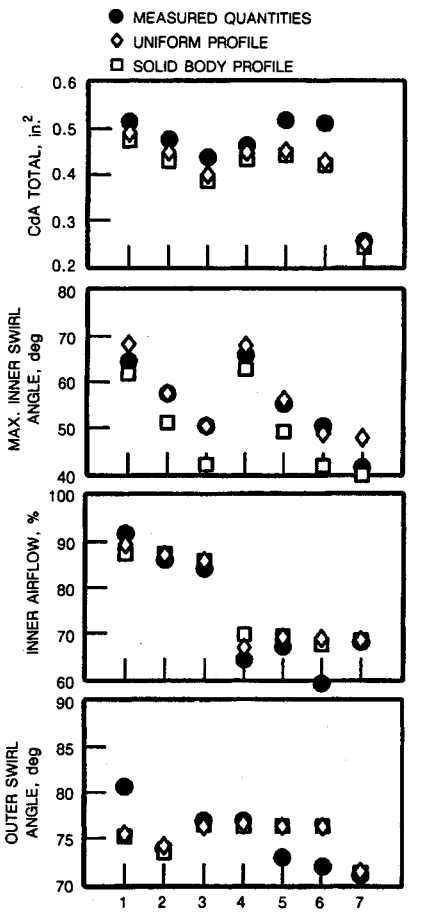

Fig. 6 Comparison of measured and calculated swirler properties.

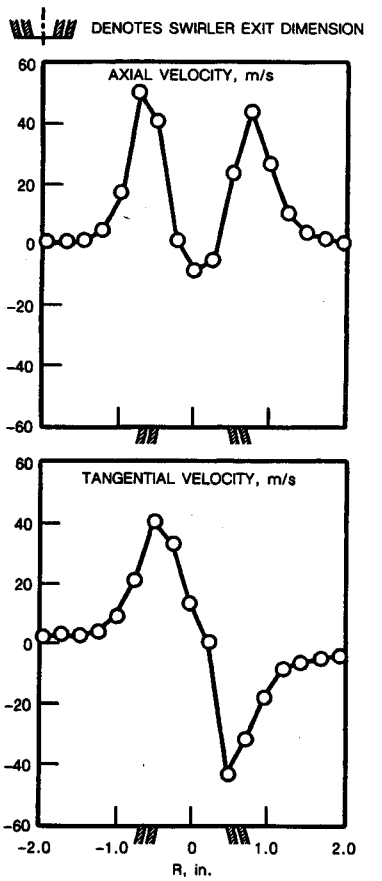

Fig. 7 Velocity profiles 1.0 in. downstream of swirler.

axial velocity and once for tangential velocity) at a downstream distance of 1.0 in. Figure 7 presents the data for these two velocity components; the boundaries of the swirler exits are also indicated. These measurements indicated that solid body rotation was a reasonable profile for the tangential velocity but that a uniform axial velocity profile was not representative. The axial velocity profile indicated the presence of a recirculation zone on the centerline; integration of the profile suggested that its outer boundary existed near r = 0.3 in.

Swirler exit profiles—as suggested by the PDPA data traverses—were used with the swirler model to obtain a third set of predictions for airflow split, swirl, and capacity. Use of linear profiles did not greatly alter the C_dA or airflow split. The inner swirl angles were significantly reduced from the solid body values, however (Table 5), by amounts ranging from 11–15 deg. These values were also notably less than those determined from the flow check. In those tests, however, the computation of swirl angle assumed that all of the pressure loss occurred at the swirler exit. The model predictions indicated that only 61–78% occurred at the exit. Using the predicted pressure loss split, a new effective exit area (C_dA^*)

Table 6 HSNS performance quality

Nozzle	No.	Swirler: Flow split, inner/outer	Swirler: Inner swirl angle, deg	Spray features: Cone angle, deg	Spray features: Mass flux, Max-Ave/Ave	Spray features: Collection efficiency
Duplex	1	85/15	60	79.1	0.267	0.76
Duplex	2	85/15	50	73.4	0.097	0.84
Duplex	3	85/15	40	62.6	0.119	0.84
Duplex	4	70/30	60	86.8	0.884	0.43
Duplex	5	70/30	50	81.0	0.361	0.66
Duplex	6	70/30	40	75.8	0.119	0.80
Duplex	7	70/30	40	53.8	0.387	0.83
Radial jet	1	85/15	60	85.6	0.411	0.70
Radial jet	2	85/15	50	77.9	0.314	0.71
Radial jet	3	85/15	40	59.2	0.199	0.80
Radial jet	4	70/30	60	87.7	0.631	0.47
Radial jet	5	70/30	50	77.9	0.275	0.76
Radial jet	6	70/30	40	61.0	0.346	0.76
Radial jet	7	70/30	40	64.6	0.466	0.77
Airblast	1	85/15	60	61.8	0.193	0.75
Airblast	2	85/15	50	47.8	0.299	0.85
Airblast	3	85/15	40	40.2	0.607	0.97
Airblast	4	70/30	60	62.9	0.355	0.78
Airblast	6	70/30	40	38.2	0.245	0.94
Airblast	7	70/30	40	33.0	0.533	0.90

was calculated. It was greater than previously obtained since only a fraction (β) of the total loss was available:

$$C_dA^*C_dA/\beta^{1/2}$$

This led to recalculated swirl angles (Table 4) which are good agreement to the linear exit profile model predictions. It then appeared that the swirler model and the flow check calculations agreed if consistent assumptions were applied. One data set obtained 1.0 in. downstream of the swirler exit, suggested that nonuniform axial and tangential velocity profiles exist at the swirler exit. Flow recirculation at the exit centerline was likely. As a consequence, the swirl angle at the primary swirler surface (the filming surface) appeared to be notably less than predicted from one-dimensional flow assumptions. Velocity data at the swirler exit are necessary to substantiate this conclusion.

Injection Technique Influence on Spray Character

Ambient spray patternation tests were performed for 21 combinations of fuel nozzle and compound radial inflow air swirler to determine the influences of fuel injection technique, airflow rate, airflow split, and swirl angle on spray pattern. Again, the inner and outer swirlers were assembled with a fixture to assure component concentricity. The nozzle bearing plate was also attached with the fixture to position the nozzle on the swirler centerline to within 0.003 in. Data were acquired 2.0 in. downstream of the swirler exit, the closest that the test fixture could be brought to the patternator. The closest position was necessary due to the wide spray cross section created by the large exit diameter of the swirler and spray cone angles. Spray patterns were analyzed to determine the configuration effects on circumferential uniformity using sector values for mass flux, spray cone angle, and overall spray quality (streaks, recirculation zones, etc.) Table 6 tabulates these results.

The most notable feature of the results for the radial jet injector was the presence of six equally spaced peaks in the spray pattern (Fig. 8). These were evident in nearly all the results, although to a greater magnitude in some. The streaks are believed to have been created by the six radial jets of the injector. These jets retained their coherency as they impinged and filmed on the swirler filming lip, causing mild streaks in the spray. However, these streaks were of nearly equal magnitude and were of a scale that was too small to be measured

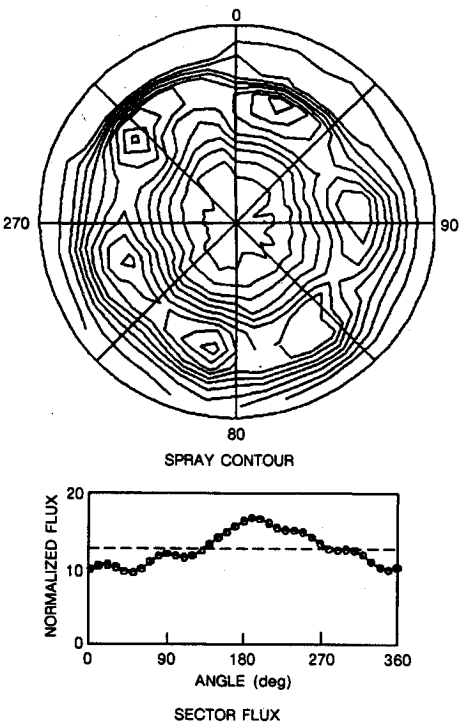

Fig. 8 Persistance of radial jet streaks in spray pattern.

through the sector analysis, which quantifies larger scale nonuniformities. That is, the plot showing the variation of sector spray flux (Fig. 8b) did not reflect six peaks. The streaks were, however, sometimes superimposed on a large scale (usually once-per-revolution) circumferential nonuniformity. When these effects produced a distribution as indicated in the figure, a (Max-Ave)/Ave value greater than deemed acceptable was attained. Spray cone angles for radial jet configurations ranged from 59.2 deg for swirler 3 to 87.7 deg for swirler 4.

The duplex pressure atomizer was also tested with all seven swirler configurations. Swirler 7 created the smallest cone angle (53.8 deg) and swirler 4, the largest (86.8 deg). Observations of the spray revealed a dual cone behavior for many configurations using the dual orifice injector. The spray cone created by the injector alone may not have been wide enough

in all cases to reach the inner filming lip of the swirler. However, smaller droplets in the spray are likely to follow airflow patterns and were carried out to the filming lip by the inner swirler airflow. This created a dual cone spray. The inner cone was created by the duplex atomizer. This cone was enveloped in a fine "veil" cone created by the smaller droplets that reached and were sheared from the filming lip.

The comparison of 90% spray cone angle for swirlers with the same design swirl angles, but different inner/outer air flow splits, also showed evidence of the spray not reaching the filming lip. For the duplex atomizer, this cone angle was considerably lower (8–13 deg) for swirlers with a high inner airflow (85%) relative to swirlers that were otherwise the same, but with a smaller inner airflow (70%). The increased axial air momentum in the high inner airflow cases is believed to keep much of the liquid fuel from reaching the filming lip. In these cases, the majority of the fuel (bigger droplets) would not reach the filming lip and the spray cone would essentially be that of the dual orifice atomizer. The spray would then cover a lower area, as it originated from essentially a point source as opposed to the filming lip. This behavior also caused the spray cone to be less hollow than a spray that would originate completely from the filming lip. Mass flux contours and radial profiles (Fig. 9) showed a broad distribution of the spray along a radius. As noted by the percentage of spray in each octant, the spray was very axisymmetric with a (Max-Ave)/Ave value of 0.097. When reasonable collection efficiencies were achieved acceptably uniform sprays were produced.

Results with the airblast injector showed that in these cases the effect of counter-rotating the swirler air and injector air was to cause the spray cone to collapse (see the three-dimensional mass flux of Fig. 10). This behavior was observed for all the swirlers tested. Swirler 7 exhibited the lowest cone angle (33.0 deg), while swirler 4 exhibited the largest (62.9 deg) although still exhibiting a center peak indicative of a collapsed cone. Information on circumferential uniformity was difficult to interpret for a collapsed cone and was also of questionable relevance.

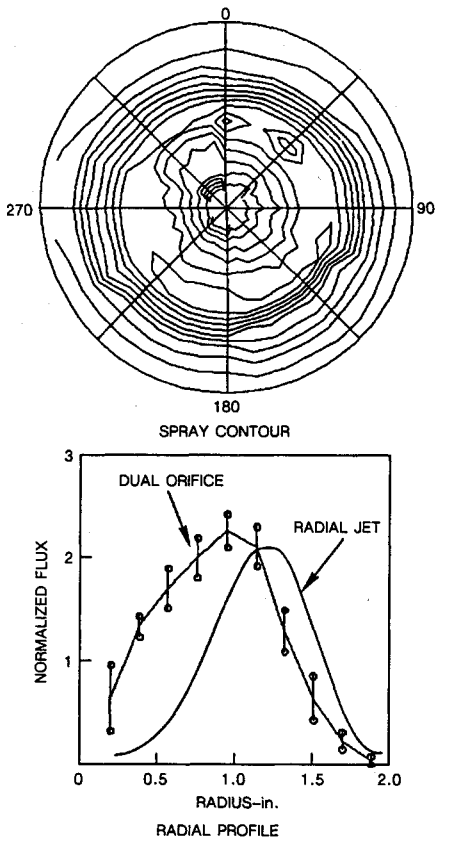

Fig. 9 Dual orifice fuel nozzle produces a more solid spray.

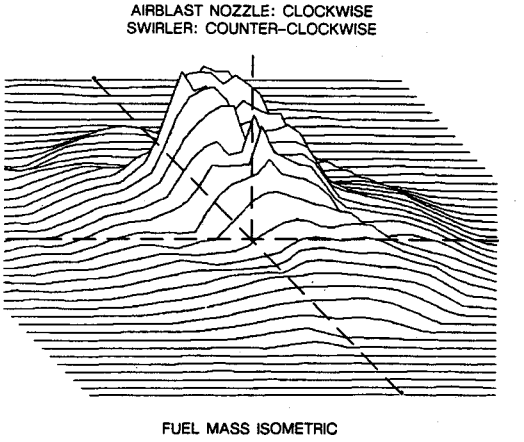

Fig. 10 Contour rotation collapsed airblast spray cone.

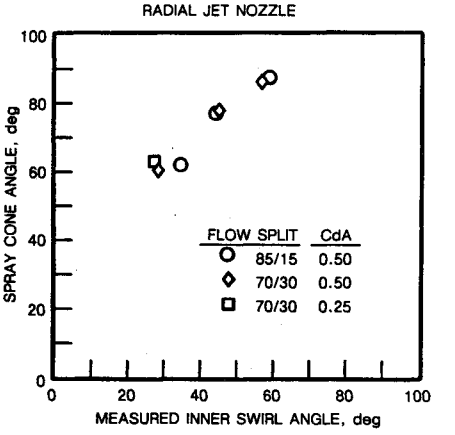

Fig. 11 Spray cone angle follows inner swirl angle.

In summary, the results from a series of tests with 21 configurations of a HSNS indicate that circumferential spray uniformity was acceptable in most cases as indicated by the computed sector fuel mass flux (Max-Ave)/Ave values (Table 6) and averaged circumferential plots. No streaks were seen, and only mild one-per-revolution large scale nonuniformities were observed. The injection technique affected the spray character according to the interaction of the liquid and air streams.

Swirler Design Influences on the Spray Character

Swirlers 1 and 4 consistently produced sprays with the largest cone angle for a given injector type. This was due to the higher swirl angles created by the inner swirler airflows in these swirlers nominally (60 deg). Swirler 7, on the other hand consistently produced small cone angles for a given injector due to its low inner swirl angle (27 deg). Spray pattern did not change significantly between swirlers with the same swirl angles but different inner/outer airflow splits. The exception to this observation was for an operation with the dual orifice injector, where the airflow split had an effect on the primary spray of the injector itself. Figure 11 shows the direct relationship of inner swirl angle on cone angle for sprays produced by the radial jet injector; in this case, fuel always filmed on the inner swirler.

When used with the two injectors which did not consistently film on the swirler—especially with the duplex nozzle—swirler 7 formed sprays with lower cone angles than swirler 6. The only design difference between these swirlers was that the effective area of swirler 7 was lower (0.25 square in.) than swirler 6 (0.50 square in.). Measurements indicated that slight differences in airflow split and inner swirl angle were also achieved. These were not significant for the radial jet nozzle (i.e., Fig. 11). It appears that an altered airflow/spray inter-

action was experienced with the duplex injector for the smaller swirler.

Results, Part 2: Manufacturing and Assembly Influences

The series of tests performed may be categorized into three groups. These focused on nozzle position (altered axial engagement, radial translation, angular alignment), air swirler exit condition (annular gap uniformity, surface imperfections) and air swirler inlet condition (blocked swirl slots, removed swirl vanes). These may be detailed as follows:

Nozzle Position

1) Baseline: nozzle and swirler axes coincident, 0.65 in. separation; and 2) variations: a) increased separation by 0.05, 0.10 in. (Fig. 12a), b) radial translation of nozzle axis by 0.05, 0.10 in. (Fig. 12b), and c) nozzle and swirler axes misaligned by 2, 4 deg (Fig. 12c).

Swirler Exit Condition

1) Baseline: circular primary exit area, uniform secondary flow annulus. No filming edge imperfections; and 2) variations: a) primary and secondary swirlers nonconcentric, annular gap (max-min) of 0.010, 0.020 in. (Fig. 13a), b) primary swirler exit ovalized to achieve annular gap (max-min) of 0.012, 0.022 in. (Fig. 13b), and c) point impression on primary swirler exit edge protruding into flow 0.010, 0.015 in. (Fig. 13c).

Primary Swirler Inlet Condition

1) Baseline: all slots in swirler equal and open; and 2) variations (Fig. 14): a) one blocked swirl slot, b) two opposed blocked swirl slots, c) one swirl vane removed, and d) four equally spaced swirl vanes removed.

Spray distributions were interpreted from the information generated from high resolution patternation data as shown in Fig. 5. The amount of liquid collected in 36 overlapping 45-deg sectors was evaluated from the patternation data. The normalized maximum deviation from the average (average for 45-deg section = 12.5% of total) denoted as (Max-Ave)/Ave was used as the indicator of circumferential uniformity. These values were normalized by the (Max-Ave)/Ave for the baseline case, yielding a relative maximum (RM). It should be noted that because of the integration of the data, small scale streaks in the spray pattern are "smoothed" out so that these data only indicate the presence of large scale uniformities. Based on the variations observed, differences of less

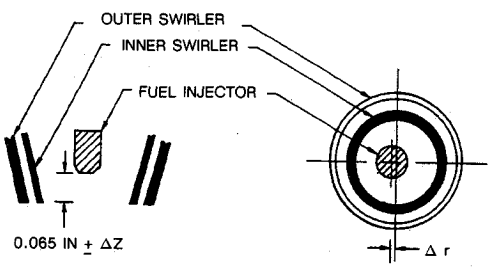

a) Axial engagement b) Radial misalignment

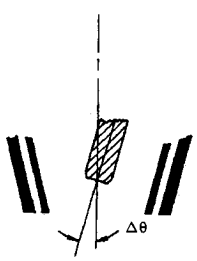

c) Angular misalignment

Fig. 12 Fuel nozzle position variations.

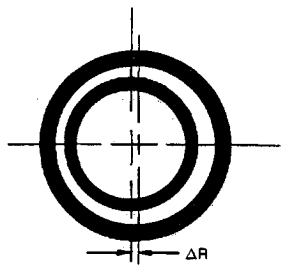

a) Inner swirler translation

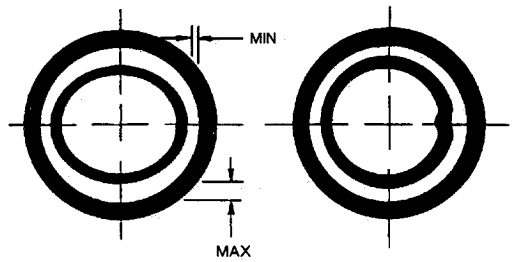

b) Inner swirler ovalization c) Point impression on fuel filming lip

Fig. 13 High-shear swirler exit variations.

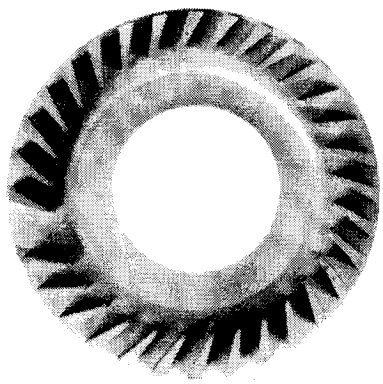

Fig. 14 Inner swirler with one vane removed.

than 0.2 between RM values were probably not significant. The radial distribution was characterized through the 90% cone angle described earlier. This cone angle, as well as (Max-Ave)/Ave and RM values are tabulated for all cases in Table 7.

The baseline case results for a properly assembled, defect-free nozzle/swirler are shown in Fig. 5. A hollow cone spray was evident, with six small equally spaced streaks easily discernible in the contour plot. These streaks reflected the six jets from the radial jet fuel injector. The mean radial profile confirmed the hollow cone characteristic with the peak spray flux occurring at a radius of 1.5 in. The "error bars" reflect one standard deviation of the 36 flux values at each radial location. The larger deviations near the peak flux were due to the mild streaks from the injector jets. These streaks were considered to be mild because they did not appear in the sector flux variation plot. A (Max-Ave)/Ave value of 0.197 also reflected a reasonably uniform spray. This is equivalently shown in the percentage of spray shown in each octant of the contour plot. In this case, the largest concentration was 14.75% of the spray, only 1.18 times the 12.5% value for a perfectly uniform spray.

Primary Swirler Inlet Alterations

The imposed alterations to the primary air swirler inlet had little or no effect on the spray pattern. The removal of one or four of the 32 swirler vanes (configurations 2 and 3 in Table 2) had a slight effect, causing a small decrease in spray cone

Table 7 HSNS performance quality

Alteration	Configuration	Cone angle, deg	Sector mass flux, Max-Ave/Ave	RM
Baseline	1	84.9	0.197	1.00
One inner swirler vane removed	2	81.1	0.239	1.21
Four inner swirler vanes removed	3	85.1	0.281	1.43
One inner swirler slot blocked	4	85.2	0.197	1.00
Four inner swirler slots blocked	5	85.8	0.168	0.85
Point impression on filming lip = 0.015 in.	6	84.7	0.251	1.27
Point impression on filming lip = 0.022 in.	7	84.9	0.194	0.98
Inner swirler ovalized: Max-Min = 0.012 in.	8	84.4	0.162	0.82
Inner swirler ovalized: Max-Min = 0.022 in.	9	84.3	0.183	0.93
Outer air gap eccentricity: Max-Min = 0.010 in.	10	84.6	0.263	1.33
Outer air gap eccentricity:	11	84.3	0.386	1.96
Radial misalignment = 0.050 in.	12	85.6	0.452	2.29
Radial misalignment = 0.100 in.	13	85.8	0.566	2.87
Angular misalignment = 2 deg	14	85.1	0.231	1.17
Angular misalignment = 4 deg	15	85.0	0.391	1.98
Nozzle engagement: DZ = 0.050 in.	16	86.0	0.412	2.09
Nozzle engagement: DZ = 0.100 in.	17	86.1	0.394	2.00

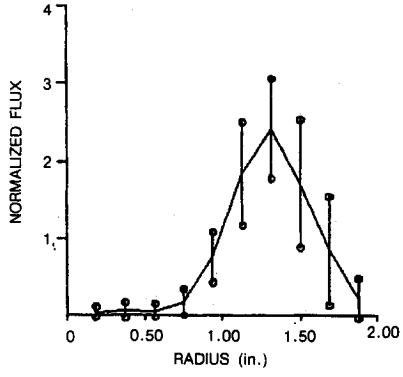

a) One vane removed

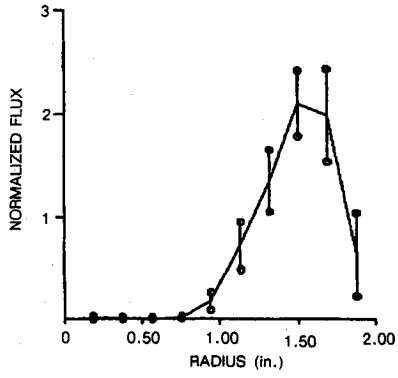

b) Baseline

Fig. 15 Spray sheath thickens with one vane removed.

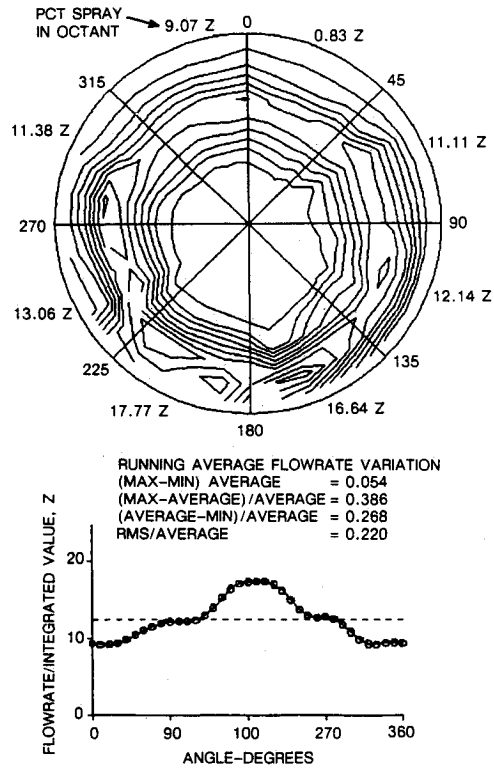

Fig. 16 Eccentricity of outer air gap causes single peak distortion of spray pattern.

angle and increasing the spray cone solidity as indicated by the mean radial profile. Figure 15 shows this effect, where one vane has been removed, causing the peak flux to shift inward and the radial profile to broaden. This may be due to an effective change in airflow split between the two passages, or to an actual nonuniformity in the spray. Blockage of one or four of the 32 swirl slots (configurations 4 and 5) had no effect on the spray distribution, as reflected by cone angles and sector mass flux quantitites essentially equivalent at the baseline values.

Swirler Exit Alterations

Point impressions of up to 0.022 in. on the fuel filming lip (configurations 6 and 7) changed the spray pattern in no significant way. Ovalization of the primary swirler exit in such a way that the difference between the maximum and minimum outer air gap height was as much as 0.022 in. (configurations 8 and 9) displayed a mild once-per-revolution variation in the sector flux, but not significantly worse than the baseline. The primary swirler was translated to create an eccentricity with the secondary swirler, producing outer air gap nonuniformities of up to 0.022 in. These changes (configurations 10 and 11) had notable effects on the patternation, especially for the largest change. In this case, the outer air gap was reduced by 30% in one direction and opened by 30% in the other. For this case, a relative maximum of RM = 1.96 was obtained, showing a significant single peak in the azimuthal distribution (Fig. 16). The magnitude of this effect is limited by the fact

that the nonuniformity is imposed only on the 15% of the airflow that passses through the annulus.

Nozzle/Swirler Alignment Alterations

Radial misalignments of the fuel nozzle and air swirler (configurations 12 and 13) had the most pronounced effects on the spray pattern. Both of these (R = 0.050, 0.100 in.) increased the single peak (i.e., once per revolution) nature of the circumferential spray distribution (see Fig. 17). The 0.10-in. misalignment increased the sector mass flux (Max-Ave)/Ave value to 0.566, yielding a relative maximum of RM = 2.87. The spray again showed a large single peak in the azimuthal distribution.

In other configurations, the nozzle was angularly misaligned so that its central axis was not parallel to that of the air swirler (configurations 14 and 15). Misalignment of 4 deg produced a small but notable change in the spray pattern. The expected bias in the fuel distribution to the filming surface changed the location of the maximum peak from near 200 deg to near 0 deg (see Fig. 18).

Nozzle engagement, measured by the distance from the nozzle tip to the swirler exit plane, was changed from the nominal value of 0.65 to 0.60 and 0.55 in. (configurations 16 and 17). The sector spray flux distribution reflected a once per revolution variation similar—but of less magnitude—to a radial nozzle displacement. The nozzle placement and angularity were tightly controlled by the assembly and mounting fixture. Hence, no explanation is offered for the engagement effect unless it was the consequence of altered two phase flow patterns within the swirler. The model airblast nozzle study[10] also concluded that the poorly understood interactions between fuel and airstreams within the device can be very important and magnify seemingly small variations.

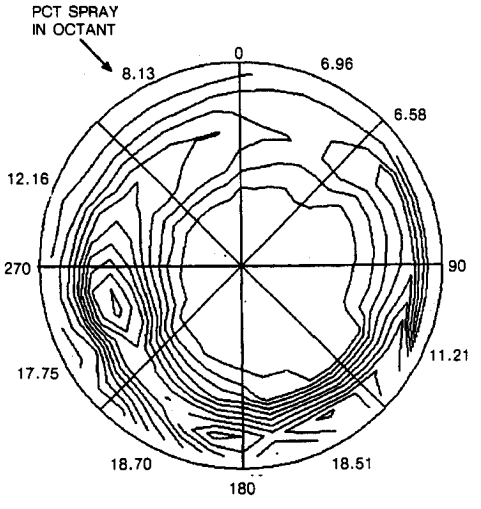

a) Spray contour

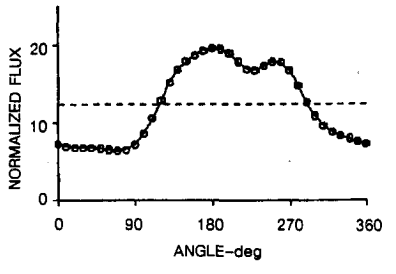

b) Sector flux

Fig. 17 Radial misalignment (0.1 in.) of fuel nozzle causes extreme single peak spray distribution.

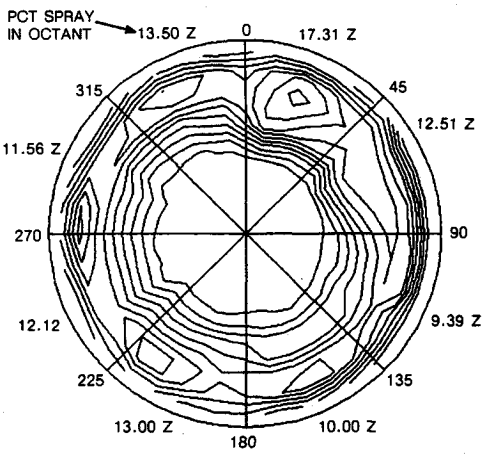

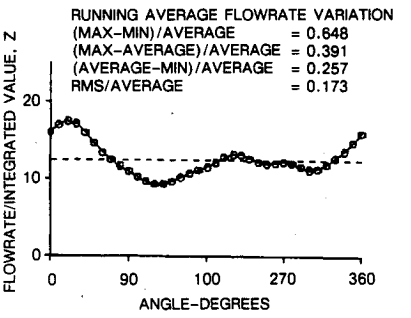

Fig. 18 Four-deg injector tilt causes single peak spray pattern.

Summary

Part 1: Design Influences

The results from a series of tests with 21 configurations of a HSNS indicated that spray distribution was more dependent on injector type rather than swirler type. This was consistent with previous results for airblast injectors[10] which showed that fuel maldistribution was one of the primary causes of circumferential nonuniformities.

Results indicated that spray cone angle was heavily influenced by the inner airflow swirl angle. High inner swirl angles created large centrifugal forces and helped to spread the spray cone radially. Low swirl angles favored a higher axial air momentum and helped to collapse the spray cone. This behavior was observed for all injectors studied.

The radial jet fuel nozzle always delivered fuel to the filming lip. Well-defined, hollow cone sprays were always produced. The fuel jets retained their coherency and created mild streaks in the spray. Their presence did not significantly compromise the spray circumferential uniformity.

The duplex injector often did not create a spray cone wide enough to reach the filming lip of the swirler. This problem was worsened by increasing the flow to the inner air swirler, and evidenced itself in the reduction of cone angle for swirlers of identical swirl strength but higher inner/outer airflow split. A dual spray cone was sometimes created by small droplets being centrifuged out to the filming lip, while larger droplets (with higher momentum) missed it. This created a "cone-inside-a-cone," the inner cone being created by the injector, and the outer cone being created by fine droplets filming off the swirler lip.

Performance with the airblast injector was poor due to the counter-rotation of the injector airflow and the swirler airflow. In the case of the test articles apparently the two flows were of comparable strength resulting essentially in only axial flow. It is believed that counter-rotating flows could be used for nozzle/swirler assemblies if one flow dominated. In this way, regions of high shear at the flow interface might be used

to enhance atomization, with the dominant swirl flow promoting fuel distribution.

The radial inflow swirler offered a convenient means to alter swirler performance parameters such as flow capacity and swirl strength. A simple mathematical model provided consistent results with experimentally determined features. Such a model cannot, however, predict the downstream flowfield. Additional analytical and experimental descriptions are required.

Part 2: Manufacturing and Assembly Influences

Spray patternation data were acquired for 17 configurations of a model HSNS. The data were analyzed to determine the effects of manufacturing and assembly influences on circumferential and radial spray mass flux distribution.

The high-shear nozzle design was insensitive to many assembly and manufacturing flaws or alterations to the air swirler. Alterations which affected the primary distribution of fuel onto the filming lip by the injector were most influential on the spray pattern.

Radial translation of the fuel injector was the most significant alteration, causing large deviations in the spray patternation from the baseline case. This nozzle/swirler concept relied upon achieving a uniform fuel film on the inner surface; radial displacement of the injector notably shifted this flux preferentially to one side of the swirler. The fueling variation and consequent spray distribution would intuitively be single-peaked, as was observed. Angular and axial misalignment of the nozzle caused less (but important) changes in the spray distribution. It was estimated that radial displacements should be less than 0.025 in. Proper angular alignment to within 3 deg should also be held.

The spray distribution was relatively insensitive to alterations which affected only the airflow. These results were consistent with those obtained in Ref. 10 for a model airblast nozzle, which demonstrates that spray pattern was more sensitive to changes in primary fuel distribution than to changes in airflow. The observation that blocking swirler slots or removing swirl vanes did not cause the spray pattern to change was consistent with results obtained in part one of this study showing that spray pattern is relatively insensitive to airflow split. That is, the effect of inlet airflow passage variations were "washed out" by the highly swirling airflow which naturally tends toward axisymmetry. It required a substantial change in the outer airflow gap to significantly alter the spray uniformity. It is estimated that the gap uniformity should be held within 0.010 in.

In conclusion, the results have indicated that restrictions must be imposed on the parameters affecting the initial distribution of fuel onto the filming surface, whereas parameters affecting only air flows are less critical. Additional study is required in determining the actual quantitative effects of nonuniform spray patterns on combustor performance.

Acknowledgments

This study was performed at UTRC under the sponsorship of the USAF WRDC Aero Propulsion and Power Laboratory, Contract F33615-85C-2515. Royce Bradley was the Program Manager. The efforts of K. Beemer, J. Grimes, and G. Fulton in the acquisition and processing of data are greatly appreciated.

References

[1]Kilik, E., "The Influence of Swirler Design Parameters on the Aerodynamic Characteristics of the Downstream Recirculation Region," Ph.D. Dissertation, Cranfield Inst. of Technology, England, UK, May 1976.

[2]Kilik, E., "Better Swirl Generation by Using Curved Vane Swirlers," AIAA Paper 85-0187, Reno, NV, Jan. 1985.

[3]Kilik, E., "Influence of the Blockage Ratio on the Efficiency of Swirl Generation with Vane Swirlers," AIAA Paper 85-1103, Monterey, CA, July 1985.

[4]Sander, G. F., and Lilley, D. G., "The Performance of an Annular Vane Swirler," AIAA Paper 83-1326, Reno, NV, Jan. 1983.

[5]Martin, C. A., "Air Flow Performance of Air Swirlers for Gas Turbine Fuel Nozzles," ASME Paper 88-GT-108, Amsterdam, June 1988.

[6]Rosfjord, T. J., and Eckerle, W. A., "Nozzle Airflow Influences on Fuel Patternation," AIAA Paper 88-3140, Boston, MA, July 1988.

[7]McVey, J. B., Kennedy, J. B., and Russell, S., "Application of Advanced Diagnostics to Airblast Injector Flows," ASME Paper 88-GT-12, Amsterdam, June 1988.

[8]McVey, J. B., Russell, S., and Kennedy, J. B., "Characterization of Fuel Sprays Using a High-Resolution Patternator," *Journal of Propulsion and Power*, Vol. 3, No. 3, 1987, pp. 202–209.

[9]Smith, C. E., Graves, C. B., and Roback, R., "Fuel Injector Characterization and Design Methodology to Improve Lean Stability," AIAA Paper 85-1183, Monterey, CA, July 1985.

[10]Rosfjord, T. J., and Russell, S., "Influences on Fuel Spray Circumferential Uniformity," *Journal of Propulsion and Power*, Vol. 5, No. 2, 1989, pp. 144–150.